Z. Kristallogr. 214 (1999) 646–651

X-ray data collection from mineral crystals by means of a position-sensitive detector: advantages and disadvantages

D. Prella*,I,II and F. Cámara II

I Università degli Studi di Pavia, Dipartimento di Scienze della Terra, Via Ferrata 1, I-27100 Pavia, Italy
II CNR Centro di Studio per la Cristallochimica e la Cristallografia (CSCC), Via Ferrata 1, I-27100 Pavia, Italy

Received October 28, 1998; accepted March 16, 1999

Abstract. In order to check for the accuracy of X-ray diffracted data collected with an area-detector diffractometer (FAST-Nonius), we have carried out several data collections on a good-quality pyrope crystal (space group $Ia\bar{3}d$; $a = 11.479$ Å) under different experimental settings and compared the results with those obtained with the same crystal mounted on a conventional Philips PW1100 diffractometer. Several parameters have been tested (detector gain, crystal-to-detector distance, frame width, integration time per image, beam intensity, shoebox size and re-measuring of overflow reflections), and four critical features of the system have been identified: the low thermal stability of the detector, its narrow dynamic range, the importance of the detector-to-crystal distance and the integration of the diffracted intensities. We are now able to select the best experimental settings in order to obtain a refinement from FAST diffraction data good as that from Philips data, in terms of R_{sym}, R_{obs} and standard deviation of the refined parameters.

Introduction

The advent of X-ray single-crystal diffractometers equipped with area detectors [e.g. multiwire, TV detector, imaging plate, Charged Coupled Device (CCD) (Arndt, 1986; Monaco, 1992)] which have been developed to alleviate the problems of data collection of macromolecular crystals (radiation damage, huge number of diffracted intensities to be measured), has given new possibilities also to small-molecule and mineralogical crystallography. Area-detector diffractometers, in fact, are the only instruments which can collect the full 3-D integration of each reflection. They are therefore potentially competitive with conventional diffractometers in the study of good-quality crystals, but very likely superior in the study of very small crystals or when there are problems such as intergrowths, polytypes, polycrystalline samples, etc. which are quite common among mineral samples.

There is an increasing number of publications about the use of PSD in the study of small molecules (e.g. Woodman, Errington, Willey, 1997; Singh, Kumar, Parmar, Errington, 1997; Burns, 1997; Kharisun, Taylor, Bevan, Rae, Pring, 1997). One paper in particular (Burns, 1998) very well demonstrates the great advantages of using the newly available CCD detector in the study of mineral crystals, expecially when they have very large cell dimensions or when the samples have very small size. However, the availability of an area detector may give further chances to a non-standard work on minerals. Single-crystal X-ray diffraction (XRD) of minerals is routinely carried out with samples selected according to their good diffraction profiles, i.e. with crystals free of inclusions, twins or defects of various nature. However, in a systematic crystal-chemical study of mineral groups, very frequently some mineral compositions cannot be characterized because of the small size of the crystals or of their low diffraction quality. This is a quite common situation in rock forming minerals. On the other hand, a huge work on mineral synthesis has been done in order to make available for crystal-chemical study some mineral compositions not present in nature. However, the experimental runs rarely provide crystal grains of suitable size and quality to perform standard XRD experiments; moreover most of these synthetic crystals show twinning or intergrowth with other product phases.

Another important application is the possibility of studying in situ intercrystalline diffusion and exchange between two mineral phases by miscellaneous collection of their diffracted intensities.

The use of a diffractometer equipped with an area detector and a high-power X-ray source (as a rotating anode) would alleviate to face all these problems. For example with such an instrument it is not difficult to identify in a short time all the mineralogical phases which are present in a rock sample and to establish the geometrical relationship between the host and the included or intergrown phases (Cámara, Prella, 1996). When all the mineral phases have been identified and their lattice parameters have been measured, X-ray diffraction data for single-crystal structure refinement of all the phases of interest can be collected in sequence.

In order to use the area-detector diffractometer to investigate specific mineralogical problems as those described before, it is necessary to optimize the experimental conditions for data collection. We have collected therefore a

* Correspondence author (e-mail: prella@crystal.unipv.it)

large number of data sets using the same crystal and changing several experimental parameters. All the data sets collected with the area detector diffractometer have been compared with the diffraction data measured with a conventional 4-circle diffractometer. The crystal used for this purpose was a good-quality pyrope crystal ($a = 11.479$ Å) from a Dora-Maira quartz-micaschists (Western Alps, Italy), which had been rounded by a grinding device in order to eliminate any problem due to X-ray absorption (a reliable absorption correction is not available in the software of the FAST or of other area-detector diffractometers).

Equipment

The area detector diffractometer tested is a FAST (Fast-scanning Area-Sensitive TV-detector diffractometer) system, equipped with a Mo rotating-anode generator (max. power 5 kW); the X-ray beam is monochromatized by a graphite crystal. The goniometer has kappa geometry and the detector is mounted on an arm with variable angle (theta) and crystal-to-detector distance. The arm has an asymmetric configuration allowing it to cover a 2θ range of 90° (from −20° to 70°).

The detector input screen is made up of a gadolinium oxysulphide (Gd_2O_2S:Tb) phosphor layer deposited on a flat fibre optics plate with 80-mm diameter, with a standard phosphor absorption of approximately 60% of MoK_α photons. The fibre optics input-plate is coupled with a DEP (Delft Electronic Products) image intensifier, the output of which is transmitted through demagnifying fibre optics to a Silicon Intensifier Target (SIT) TV-tube. The image is scanned 25 times per sec, and the amplified signal is digitalized with a spatial resolution of 512 × 512 pixels (8-bit resolution each). The sensitivity of the detector can be varied to accommodate (nominally) a wider range of beam intensities.

The whole system is controlled by the software MADNES (Munich Area-Detector New EEC Software; Messerchmidt, Pflugraft, 1987) running on a DIGITAL microVAX 4000-400 computer.

The single-crystal diffractometer equipped with a conventional scintillator counter is a 4-circle diffractometer Philips PW1100; it works in Eulerian geometry and is controlled by a highly improved local version of the original Philips software. The X-ray source is a graphite-monochromatized Mo sealed-tube usually working at 1.5 kW (60 kV × 25 mA). Both the instrument and the software for data collection via profile-fitting methods have been used many times in recent years, obtaining very fast data collections and very high accuracy of the integrated intensities.

Experimental procedures

With the Philips diffractometer each reflection is measured in a traditional way using the Lehmann and Larsen method (1974); if the intensity is lower than a threshold the reflection is measured again for a number of time fixed in advance. In the data collection used as reference, the $\omega/2\theta$ scan type was chosen, with a scan width of 2.4° in ω and a speed of 0.12 °/sec. With the FAST system, there is no well-assessed procedure to collect diffraction data on a mineral sample; therefore, all the following parameters have been tested: detector gain, crystal-to-detector distance, frame width, integration time per image, beam intensity, shoebox size and re-measuring of overflow reflections. The performance of the diffractometer with the default values of each parameter was checked during the PhD thesis of Prella (1996), and the results will not be discussed here. The present diffraction data were collected with different frame widths (fw = 0.4°, 0.2°, 0.1° and 0.05°), detector gain (dg = 73.62, 58.28, 45.24, 32.68, 21.22, 10.98, 4.2 msu/fixel), shoebox size (ss = 31 × 31, 21 × 21, 15 × 15 pixels), generator power (gp = 3000, 2250, 1500 W) and frame integration time (fit = 30, 15 sec). These experiments showed that the best results (in terms of R_{sym}, R_{obs} and esd of the refined parameters) could be obtained using fw = 0.1°, DG = 45.24 msu/fixel, ss = 15 × 15 pixels, gp = 3000 W and fit = 30 sec. In particular, we noticed that R_{sym} and R_{obs} were improving with decreasing fw values; we chose 0.1° as the best compromise between the quality of the data and the time devoted to data collection. As regards generator power and integration time, they should be chosen so as to provide the best counting statistics on the measured intensities. If the generator power is too high, the counting statistics on weak reflections are better; however the number of overflow reflections proportionally increases, and this strongly reduces the number of reflections present in the data set. On the contrary, when the integration time increases, weak reflections improve and the number of overflow reflections does not increase. For the present crystal, 30 sec. of integration time were enough to obtain good counting statistics on a large proportion of weak reflections.

Results

The present work allowed us to identify four critical features of the FAST system: the thermal stability of the detector, its narrow dynamic range, the importance of the detector-to-crystal distance and the integration of the diffracted intensities. These will be briefly discussed in the following.

Thermal stability of the detector

The variation of the detector readout is controlled by: 1) the intensity of the β-lights (three phosphor-coated glass-vials containing tritium, placed at three corners of the area detector); 2) the variation of the detector dark current (DC; i.e., the TV-camera temperature-dependent output signal). The correction for DC variation is done using a factor (DCfact) which is calculated as the ratio between a reference DC and the DC in every image. The reference DC is an image registered with the shutter closed (DARK image) at the beginning of the data collection.

We have verified that both these parameters are highly sensitive to variations in the detector temperature. There-

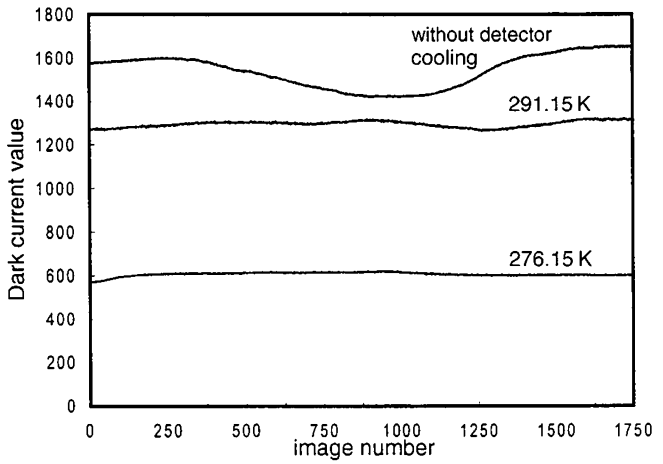

Fig. 1. Changes in the dark current during data collection under different detector temperatures.

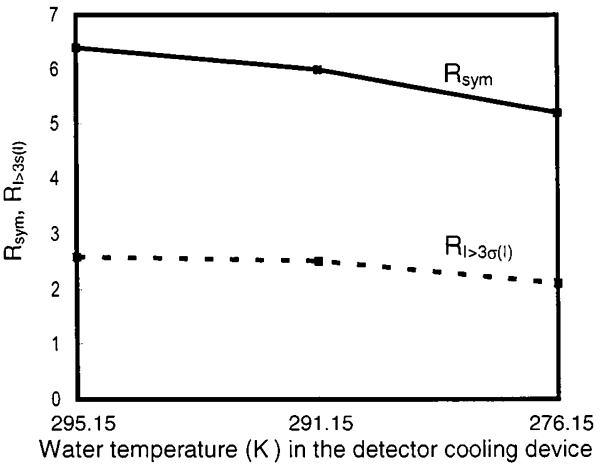

Fig. 2. Changes in R_{sym} and R_{all} for three different temperatures of the water cooling the detector.

fore, it was compulsory to stabilize the detector temperature by sucking air in the back of the detector through a big block of aluminium which works as a heat exchanger. In order to improve the thermal stability and to obtain a more stable background signal (DC) we cooled the aluminium block with a water flux at a temperature controlled by a cryostat. We tested this parameter by working at two different temperatures, namely 291.15 K and 276.15 K. The behaviour of the DC during a data collection with and without detector temperature control is shown in Fig. 1. Without water cooling, the detector temperature variations were high enough to cause stoppage of data collection ($\Delta\beta$-light >10%). In the presence of water cooling, the DC variation was significantly reduced resulting in a more stable response.

The X-ray data set collected after temperature stabilization of the detector shows a clear improvement (Table 1; Fig. 2). The further improvement going from 291.15 K to 276.15 K is not so crucial for a strongly diffracting sample such as the pyrope crystal; it might be important in the case of less diffracting crystals, the background being much lower and more stable at the temperature of 276.15 K.

In the latest generation of CCD detectors, the problem of temperature control has been solved by the factory. The high compactness and robustness of the CCD hardware permits cooling of the chip to very low tem-

Table 1. Experimental conditions and refinement results of X-ray diffraction data collected with: detector cooled at different temperatures (FAST1-2-3), high generator power and the standard re-measuring procedure (FAST4), two different generator powers (FAST 5a) or two different detector sensibilities (FAST 6a); in FAST 5a and FAST 6a the two data sets have been merged. *T*, *Y*, *X* are the cationic sites of the garnet structure with number of coordination 4, 6, 8, respectively.

	Philips	FAST 1	FAST 2	FAST 3	FAST 4	FAST 5a	FAST 6a
detector temp. (K)		295.15	291.15	276.15	276.15	276.15	276.15
gen. pow. (W)	1500	1500	1500	1500	3500	3500 & 700	3500
sw-fw (°)	0.01	0.10	0.10	0.10	0.10	0.10	0.10
scan rate (°/sec)	0.070	0.003	0.003	0.003	0.003	0.003	0.003
dct (h)	22	34	34	34	34	34	34
dx (mm)	190	32	32	32	32	32	32
sin θ/λ max. ($Å^{-1}$)	0.82	0.82	0.82	0.82	0.82	0.82	0.82
detector sensibility		5, 7	5, 7	5, 7	5, 7	5, 7	5, 7 & 1, 1
$n°$ of measured refl.	2667	4246	4950	4950	4659	4926	4857
R_{sym} (%)	4.3	6.4	6.0	5.2	4.8	6.0	5.4
$R_{I>3\sigma}$ (%)	1.85	2.58	2.51	2.11	2.41	2.39	2.02
Refl. with $I > 3\sigma(I)$	297	343	353	353	363	375	375
R_{all} (%)	3.15	3.31	2.88	2.89	2.95	2.80	2.45
$n°$ of indip. refl.	397	384	392	385	377	396	396
T–*O* (Å)	1.635(1)	1.634(1)	1.635(1)	1.634(1)	1.635(1)	1.634(1)	1.634(1)
Beq *O* ($Å^2$)	0.53(1)	0.35(1)	0.44(1)	0.40(1)	0.36(1)	0.41(1)	0.42(1)
Beq *T* ($Å^2$)	0.34(1)	0.17(1)	0.23(1)	0.21(1)	0.18(1)	0.22(1)	0.23(1)
Beq *Y* ($Å^2$)	0.36(1)	0.16(1)	0.27(1)	0.20(1)	0.19(1)	0.29(1)	0.31(1)
Beq *X* ($Å^2$)	0.71(1)	0.54(1)	0.58(1)	0.53(1)	0.54(1)	0.64(1)	0.64(1)
ss *Y* ($n°$ of elect.)	13.00	12.85	13.09	12.90	12.93	13.17	13.21
ss *X* ($n°$ of elect.)	13.66	13.70	13.69	13.49	13.65	13.92	13.91
GOF	1.2384	1.5998	1.5560	0.9800	1.4235	1.4562	1.1964
$n°$ of data sets			1	1	1	2	2

Note: sw = scan width; fw = frame width; dct = data collection time; dx = crystal-to-detector distance; *T*, *Y*, *Z* = sites of the garnet structure; ss = site scattering.

peratures (about 216.15 K). The electronics of CCD detectors are thus much more stable than those of the TV detector.

Dynamic range

The maximum output signal of the SIT camera tube is a current of 300 nA, which is converted to a voltage of −2 Volts. The digitalization of this signal by the eight-bit analogical-to-digital converter (ADC) of the FAST detector gives the number 255. Therefore the ADC can count up to 255 ADU (Analogical Digital Units) every 40 msec. Because 4 ADU = 1 MSU (Mass Store Unit), during an integration of 0.16 seconds the pixels in the mass store with counts greater than 255 are saturated. The maximum possible counts for an integration of t seconds is therefore 255*(t/0.16). This ADC-overflow, which is a camera overflow, restricts the dynamic range in the region of strong reflections, which cannot be well measured at high detector sensibilities. The lower limit of the dynamic range depends on the control of the background.

The effective dynamic range of the FAST detector for a single gain value has been measured to be about 1000:1. This is not enough for mineralogical studies because the dynamic range of the diffraction pattern (i.e., the ratio between the strongest and weakest diffracted intensities in a diffraction pattern) of mineral crystals is much wider than that of protein crystals; therefore, there will be less reflections correctly evaluated for each setting of the detector gain. When the detector gain is high, weak intensities are well measured, but there will be too many strong reflections that saturate the detector (overflow reflections); when it is low, many weak reflections will not have statistically significant values. We found that the latter problem can be reduced by keeping the detector at a low and constant working temperature; this significantly reduces the background and makes the signal much more stable.

The former problem can be only partially solved in the FAST system by an automatic re-measuring procedure. During the data collection, every time a single pixel is saturated the image is recollected using a lower gain; then the new mass-store intensity is scaled with the original image, the scale factor being the ratio of the gains of the two images. The gain values have been selected at the factory, and the user can only choose one of them for the re-measuring procedure. Each gain value corresponds to a specific setting of the detector parameters (high voltage of the image intensifier, high voltage of the camera amplifier) that define its sensibility. Unfortunately, the maximum dynamic range provided by the remeasuring procedure is not large enough to accurately determine the intensity of the strongest and weakest reflections diffracted from the same crystal. Moreover, with this procedure the sensibility of the detector is continuously changing during the data collection, as nearly all the images contain some strong reflections. This implies an additional instability on the detector electronics. The final result is a significant decrease in the atomic displacement parameters (adp's) in respect to the values obtained in the refinement of "conventional" diffractometer data, since the strongest reflections still saturate the detector. The loss of intensity of the strongest reflections is somehow compensated during the SREF procedure by an increase of the scale factor; however it produces an increase of the structure factors also of the weak reflections whose number largely increases with increasing θ. As a consequence, SREF gives adp's lower than the correct ones.

We found that the best results can be obtained by doing two data collections with two different powers applied to the generator or with two different gains, and then scaling and merging both sets of data. With this procedure, the dynamic range of the detector greatly increases (the ratio between the strongest and the weakest intensities is about 5.000.000:1) and we can measure with good accuracy both strong and weak reflections. We thus obtain lower R-factors and higher adp's. However, the latter are still lower than those obtained with the conventional diffractometer (Table 1).

The analogic-to-digital converter of the Nonius KappaCCD is a 16-bit ADC that can count up to 2**16 − 1 (the sign bit). Therefore the dynamic range of the CCD is bigger then that of a TV-detector, but only at one gain value. In fact the total dynamic range is bigger in the TV-detector.

Crystal-to-detector distance

In order to collect high-resolution data (up to $\sin\theta/\lambda = 0.9$ Å^{-1}) with a single detector setting we need to work at the shortest crystal-to-detector distance (DX) allowed by the hardware, i.e. 32 mm.

Therefore we checked the influence of DX on the quality of the collected data. As DX increases, the R_{sym} value decreases and a similar, although less evident, trend is observed for the refinement R-factors. Moreover, at increasing DX the adp's and the other parameters become closer to those obtained with a scintillator-counter diffractometer (Table 2).

A possible explanation of this behaviour is related to the way in which the software integrates the reflections and corrects for spatial distortion.

Spatial distortion, i.e. distortion in the geometry of the detected image, is due to the characteristic of the detector hardware (especially of the image intensifier) and to the fact that the detector is a flat surface on which we project a section of the Ewald sphere the curvature of which is an inverse function of DX. In the FAST detector, calibration for spatial distortion is made by putting in front of the detector surface a hexagonal grid of transparent holes. This grid is irradiated by a fluorescent scatterer (Y for MoK_α; Fe for CuK_α) to produce a known pattern on the detector. The difference between the ideal position of each hole and its observed position is determined, and distortion factors for each pixel are calculated by polynomial coefficients. Although this procedure allows improvement of the data, the reflections falling at the border of the detector cannot be corrected satisfactorily at the very short distance of 32 mm.

The spread of the diffracted spot is also directly proportional to the detector-to-crystal distance. The integration

Table 2. Experimental conditions and refinement results of X-ray data collected with different crystal-to-detector distances (DX). *T*, *Y*, *X* are the cationic sites of the garnet structure with number of coordination 4, 6, 8 respectively.

	Philips	FAST 5a	FAST 5b	FAST 5c	FAST 6a	FAST 6b	FAST 6c
detector temp. (K)		276.15	276.15	276.15	276.15	276.15	276.15
gen. pow. (W)	1500	3500 & 700	3500 & 700	3500 & 700	3500	3500	3500
sw-fw (°)	0.01	0.10	0.10	0.10	0.10	0.10	0.10
scan rate (°/sec)	0.070	0.003	0.003	0.003	0.003	0.003	0.003
det (h)	22	34	68	102	34	68	102
dx (mm)	190	32	60	80	32	60	80
sin θ/λ max. ($Å^{-1}$)	0.82	0.82	0.82	0.82	0.82	0.82	0.82
detector sensibility		5, 7	5, 7	5, 7	5, 7 & 1,1	5, 7 & 1, 1	5, 7 & 1, 1
$n°$ of measured refl.	2667	4926	3743	3923	4857	3729	3825
R_{sym} (%)	4.3	6.0	4.5	4.1	5.4	3.9	3.6
$R_{I>3\sigma}$ (%)	1.85	2.39	2.22	1.85	2.02	2.26	2.02
Refl. with $I > 3\sigma(I)$	297	375	379	354	375	382	357
R_{all} (%)	3.15	2.80	2.40	2.62	2.45	2.65	2.56
$n°$ of indip. refl.	397	396	396	374	396	398	374
T–*O* (Å)	1.635(1)	1.634(1)	1.634(1)	1.634(1)	1.634(1)	1.634(1)	1.634(1)
Beq *O* ($Å^2$)	0.53(1)	0.41(1)	0.55(1)	0.50(1)	0.342(1)	0.58(1)	0.54(1)
Beq *T* ($Å^2$)	0.34(1)	0.22(1)	0.33(1)	0.31(1)	0.23(1)	0.34(1)	0.34(1)
Beq *Y* ($Å^2$)	0.36(1)	0.29(1)	0.37(1)	0.34(1)	0.31(1)	0.38(1)	0.39(1)
Beq *X* ($Å^2$)	0.71(1)	0.64(1)	0.70(1)	0.68(1)	0.64(1)	0.70(1)	0.73(1)
ss *Y* ($n°$ of elect.)	13.00	13.17	13.10	13.09	13.21	13.09	13.13
ss *X* ($n°$ of elect.)	13.66	13.92	13.75	13.72	13.91	13.7	13.85
GOF	1.2384	1.4562	1.1639	0.9319	1.1964	1.2011	1.1143
$n°$ of data sets		2	4	6	2	4	6

Note: sw = scan width; fw = frame width; det = data collection time; dx = crystal-to-detector distance; *T*, *Y*, *Z* = sites of the garnet structure; ss = site scattering.

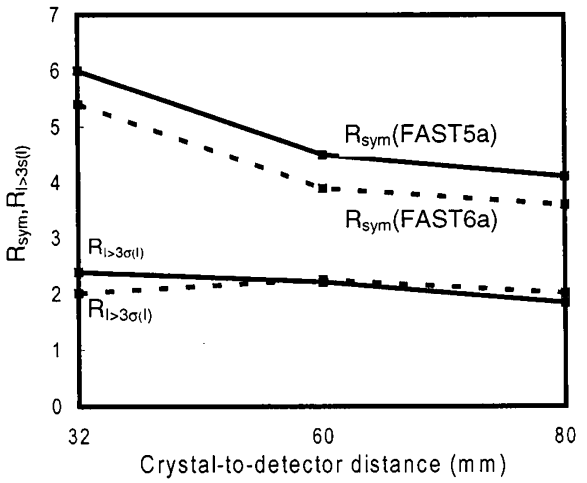

Fig. 3. Changes in R_{sym} and R_{all} as a function of crystal-to-detector distance for scaled data-sets collected with different generator power (line) or detector sensibility (dotted line), the data are reported in Table 2.

procedure works quite well with diffuse reflections but not with sharp reflections which cannot therefore be correctly integrated.

Fig. 3 is a plot of R_{sym} and $R_{I>3\sigma(I)}$ vs. DX. It is worth to note that R_{sym} values are lower when two different detector sensibilities are used instead of different beam powers.

Integration of the intensities

The evaluation software provided by MADNES is based on the work of Wilkinson, Khamis, Stansfield, McIntyre (1988); it determines the three-dimensional profile of each reflection by using a best-fit ellipsoid. This method is more time saving than a complete integration of the real reflection profiles without *a priori* information and, therefore, is very useful in the case of macromolecular crystals, which usually have reflections with a very regular although broad profile (depending on the shape of the crystal and the quantity of solvent). On the contrary, mineral crystals most often show reflections with an irregular shape. In this case the best-fit ellipsoid cannot provide a correct integrated intensity. It often happens that the volume of the reflections is larger than the maximum elliptical volume allowed by the software; in these cases, the integrated intensity is considerably lower as part of the reflection is considered as background (and thus even subtracted to the raw intensity). We have realized this problem during the observation of some on-line data collection on samples with two or more equivalent planes diffracting in the same group of frames. In this case, we obtained very frequently two equivalent reflections with a large difference in the integrated intensity. Even if a warning message appears, saying that a reflection is bigger than the maximum volume, the assigned error code is that of a reliable reflection.

Evaluation software with which to integrate the real three-dimensional profile of each node of the reciprocal lattice without a-priori modelling of the shape of the reflections would be fundamental to improve the capability of the area detector to investigate problems typical of mineral samples. This improvement would be particularly important for low-quality crystals. It would surely produce a significant increase of both the time used to integrate the intensities and the memory requirements of the computer.

However, time is not an important factor if the solution of complex mineralogical problems as exsolutions and intergrowths are attained, and the rapid development of more powerful computers would provide more memory at reasonable price.

Conclusions

In spite of several critical points, area-detector diffractometers, both with CCD counter (Burns, 1998) and with TV detector, can be now considered competitive with conventional-counter diffractometer also in the field of crystal-chemical studies of minerals; however, further improvement is needed. In any case, these new instruments provide the advantage of giving a complete picture of the diffracted intensities, thus allowing the intensity diffracted by problematic or imperfect crystals to be confidently measured and minor phases (which are present as exsolution lamellae or as inclusions) to be identified. Moreover, although data collection time for minerals with small unit cell volumes can be somewhat longer with a TV detector, it gives a better estimation on weak reflections, and a complete 3D integration gives better $I/\sigma(I)$ than a single profile, which is the method used with conventional counters. In addition, the X-ray data set collected by area detector always contains many redundant reflections (symmetry-related reflections or reflections measured more than one time during the data collection). The redundant reflections (see Table 1) improve the statistics of the data, thus giving a higher number of "observed" reflections ($I > 3\sigma(I)$).

References

Arndt, U. W.: X-ray Position-Sensitive Detectors. J. Appl. Crystallogr. **19** (1986) 145–163.

Burns, P. C.: A new uranyl oxide hydrate sheet in vandendriesscheite: implications for mineral paragenesis and the corrosion of spent nuclear fuel. Am. Mineral. **82** (1997) 1176–1186.

Burns, P. C.: CCD area detectors of X-rays applied to the analysis of mineral structures. Can. Mineral. **36** (1998) 847–853.

Càmara, F.; Prella, D.: X-ray analysis of a polycrystalline mica sample with an area detector diffractometer. 76° Meeting S.I.M.P., Bologna 1996.

Kharisun; Taylor, M. R.; Bevan, D. J. M.; Rae, A. D.; Pring, A.: The crystal structure of mawbyite, $PbFe_2(AsO_4)_2(OH)_2$. Mineral. Mag. **61** (1997) 685–691.

Lehmann, M. S.; Larsen, F. K.: A method for location of the peaks in step-scan-measured Bragg reflections. Acta Crystallogr. **A30** (1974) 580–584.

Messerschmidt, A.; Pflugrath, J. W.: Crystal orientation and X-ray pattern prediction routines for area-detector diffractometer system in macromolecular Crystallography. J. Appl. Crystallogr. **20** (1987) 306–315.

Monaco, H. L.: Experimental methods in X-ray crystallography. In: *Fundamentals of Crystallography* (Eds. C. Giacovazzo), p. 229–318. Oxford Science Publications 1992.

Prella, D.: Studio cristallografico di minerali delle rocce mediante area detector. PhD Thesis (1996) 107.

Singh, A.; Kumar, R.; Parmar, V. S.; Errington, W.: 6-Hydroxy-5,7-dimethoxy-4-methyl-coumarin. Acta Crystallogr. **C53** (1997) 1966–1968.

Wilkinson, C.; Khamis, H. W.; Stansfield, R. F. D.; McIntyre, G. J.: Integration of single-crystal reflections using area multidetectors. J. Appl. Crystallogr. **21** (1988) 471–478.

Woodman, T. J.; Errington, W.; Willey, G. R.: Polymeric Aquatri-μ-chloro-(tetrahydrofuran-*O*)lanthanum(III). Acta Crystallogr. **C53** (1997) 1801–1803.